IEEE Robotics and Automation Letters (RAL) paper presented at the
2020 IEEE/RSJ International Conference on Intelligent Robots and Systems (IROS)
October 25-29, 2020, Las Vegas, NV, USA (Virtual)

Low-cost Coil-shaped Optical Fiber Displacement Sensor for a Twisted and Coiled Polymer Fiber Actuator Unit

Ken Masuya[1]

***Abstract*— This study proposes a low-cost coil-shaped optical fiber (COF) sensor that can be used in the twisted and coiled polymer fiber (TCPF) actuator unit. The TCPF is a thermal-driven artificial muscle with large stroke and large power ratio. To improve its response, several actuator units, which combine the TCPF with a cooling system, were developed. However, the displacement sensors for these units were not established, unlike the encoder for the motor. Although several methods are available to estimate the TCPF displacement, they are based on the resistance of the heating wire and are affected by TCPF actuation and load change. Therefore, to accurately measure displacement, in this study, we focus on the bending loss of optical fiber, which is often used in soft robotics. Because the bending loss of COFs is caused by the change in length of the coil, the displacement can be obtained by measuring the light intensity through the optical fiber. This study experimentally demonstrates that the COF is available, even when driving the TCPF actuator and changing the load.**

I. Introduction

Soft robots are expected to operate in proximity to people, and soft actuators play an important role in realizing such robots. A type of soft actuator that has recently gained attention is obtained by heating twisted polymer fiber (TPF) [1]. Based on the motion, this actuator is classified into two types: rotation type and translation type. Because of the different fabrication processes, the former and the latter types are called TPF actuator and twisted and coiled polymer fiber (TCPF) actuator, respectively. This study focuses on the TCPF actuator. The TCPF actuator can output large force per mass and has large stroke, and both it is lightweight and relatively cheap. However, its response is slow because it is a thermal-driven actuator.

Conventional approaches to improve the response are roughly divided into two approaches. One is changing the nature of the TCPF actuator itself [2], [3], [4], and the other is unitizing the TCPF actuator with a cooling system [5], [6], [7], [8]. Although the former approach mainly focuses on the material and the structure of the fiber, this approach is difficult to apply to other existing TCPF actuators. Meanwhile, as the latter approach is available to other TCPF actuator, this letter focuses on this approach.

One way of cooling the TCPF actuator is via liquid cooling [5], [6]. A thermal-drive system that uses water in both the heating and the cooling phases was unitized by Wu et al. [5]. Furthermore, Song and Hori [6] proposed an actuator unit that employs liquid cooling in the cooling phase and Joule heating in the heating phase. Although liquid cooling is beneficial for improving the response, a liquid cooling system comprises liquid, pump, and reservoir, making it heavy. Conversely, air-cooling systems could be lighter than liquid-cooling systems. Yip and Niemeyer [7] developed a robotic hand comprising a TCPF actuator and a cooling fan. Takagi et al. [8] proposed a controller switching Joule heating and air-cooling. However, those units rely on external sensors, such as the laser range sensor, for feedback control. Therefore, this study focuses on developing a displacement sensor that can be incorporated with an actuator unit, similar to an encoder for electrical motors.

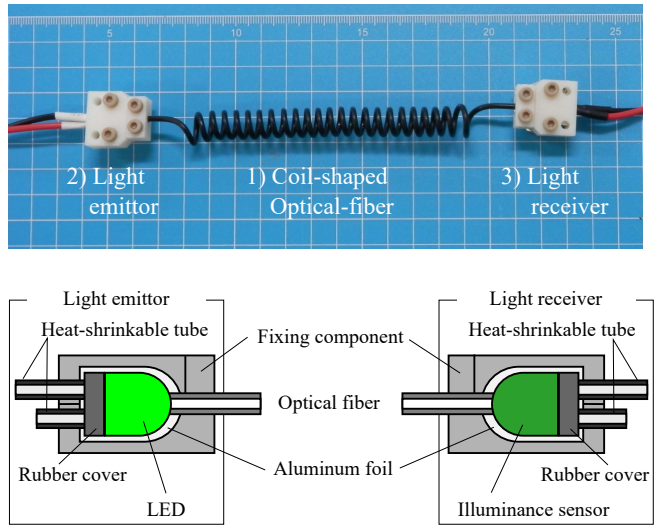

Fig. 1. Developed coil-shaped optical fiber sensor.

As a measuring method for the TCPF actuator, the electrical properties of wire for heating are often utilized; one such property is the electrical impedance of wire [9]. Because this measuring method requires an LCR meter to obtain the impedance, it is not suitable for an actuator unit. Another property is the resistance of a wire. Abbas and Zhao [10] proposed a theoretical model of the TCPF actuator, and they developed a soft curvature sensor [11]. Although their model shows good results under constant temperature, it does not consider the effect of its actuation. For the TPF actuator, a displacement estimator based on the resistance-temperature and temperature-displacement model has been proposed [12], [13]. Although this method has been validated to work under actuation, the constant load is premised. The controller based on the electrical impedance of the wire [14] has the same limitation as well. Furthermore, in these methods, it is difficult to address the load-dependent hysteresis reported by Zhang et al.[15] and the temperature-dependent hysteresis by

[1]Ken Masuya is with the Department of Mechanical Engineering, School of Engineering, Tokyo Institute of Technology, 2-12-1 Ookayama, Meguro-ku, Tokyo, Japan ken.masuya[at]ieee.org

Tanizaki et al. [16]. This indicates that an air-cooling system with a temperature sensor, such as [17], suffers from these hysteresises when controlling the displacement. Although Xiang et al. [18] designed a hysteresis model based on the Prandtl-Ishlinskii model, this model does not consider the load change. Zhang et al. [15] considered the load change, but their model requires prior knowledge of the current load. Bombara et al. [19] investigated the former hysteresis and proposed a displacement sensor for the twisted string actuator using TCPF. However, applying this method to a TCPF actuator is difficult because this method was modeled under constant temperature. Thus, the problem caused by the hysteresis remains when driven the TCPF actuator.

Meanwhile, optical fibers are often utilized as the sensor for soft robots. Although the FBG sensor [20] is one option to use the optical fiber, its measurement cost invalidates the low-cost feature of the TCPF actuator, which is one of its important advantages. Moreover, Wakimoto et al. [21] developed an optical fiber displacement sensor for the pneumatic artificial muscle. This sensor is based on the bending loss of light caused by the displacement change [22], and this loss can be measured by a low-cost illuminance sensor. However, as the temperature change affects the light through the optical fiber, whether the optical fiber sensor can be incorporated with the TCPF actuator unit remains an issue.

Based on the idea of bending loss, this study proposes a coil-shaped optical fiber (COF) sensor to measure the displacement of the TCPF actuator. The developed COF sensor is shown in Fig. 1. In displacement sensing, this sensor is connected to the TCPF actuator in parallel. Although the structure of the sensor is similar to that of [21], [22], this is the first study addressing the availability of the COF sensor for the TCPF actuator. The main contribution of this study is to investigate the utility of this sensor when driving the TCPF actuator and changing the load.

This letter is structured as follows. Section II details the developed COF sensor and its electrical circuit for implementation. Section III establishes a practical model of the COF displacement sensor via a measurement experiment. Section IV presented the conducted displacement control experiments to validate that the sensor works when driving the TCPF actuator and changing the load. Finally, Section V presents the conclusion and future work.

II. Coil-shaped optical fiber sensor

A. Developed coil-shaped optical fiber sensor

Optical fiber is a candidate for developing sensors for soft robots [20], [21]. To measure the displacement of the McKibben pneumatic muscle, Wakimoto et al. [21] replaced a sleeve fiber with an optical fiber, i.e., the optical fiber is formed in a coil shape. In their sensor, changing the length of the coil causes the curvature of the optical fiber to change; this curvature change decreases the intensity of light propagating through the fiber [22], [23]. This change in light intensity can be measured by an illuminance sensor, thereby revealing the displacement.

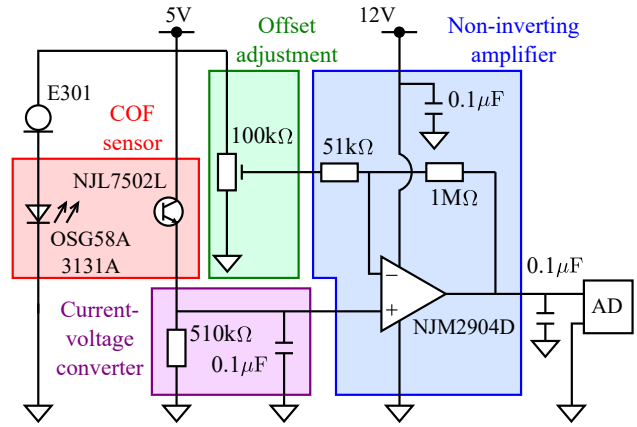

Fig. 2. Electrical circuit for the developed optical fiber sensor

Although the COF sensor developed herein is based on the same principle, it is not embedded in the actuator structure, unlike that in Wakimoto et al.[21] The smatic of the developed COF sensor is shown in Fig. 1. This sensor is composed of three parts: COF, light emitter, and light receiver. First, to prevent the incidence of light from the surrounding environment, a polyethylene-coated optical fiber was used. To realize the coil shape of the optical fiber, the optical fiber was heated at 70°C for 10 min by an automatic oven (DOV-450, AS-ONE) after winding it onto a mandrel. Second, to form the light emitter, an LED (OSG58A3131A, OptoSupply) and the optical fiber were fixed by sandwiching them between two fixing components made of acrylonitrile butadiene styrene resin. To reduce the dissipation of light to the environment, we wrap the LED and the end of the optical fiber with an aluminum foil. Third, the same method used in the second part is employed to fix an illuminance sensor (NJL7502L, New Japan Radio Co., Ltd.) and the optical fiber. Because the illuminance sensor is affected by light from the environment, the illuminance sensor and the fiber end are wrapped with an aluminum foil, similar to that performed for the light emitter. Additionally, a rubber cover is employed to reduce light from the gap between the wires.

B. Electrical circuit for the proposed sensor

To measure the output signal by the AD converter, the output current of the illuminance sensor must be converted into voltage. However, the raw voltage change caused by a change in length is minuscule to be used in the controller; thus, voltage amplification is required. Although the current–voltage converter, which is a standard photodiode application, can work as the voltage amplifier, its amplification factor is limited owing to the offset voltage. Therefore, the amplifier with offset adjustment is necessary.

Fig. 2 shows the electrical circuit of the developed COF sensor. After converting the output current of the illuminance sensor into voltage, the voltage is amplified using a non-inverting amplifier with offset adjustment. To stabilize the operation of the LED, we employ a current regulation diode. The total cost of the developed COF sensor and its electrical circuit is less than 1000 JPY.

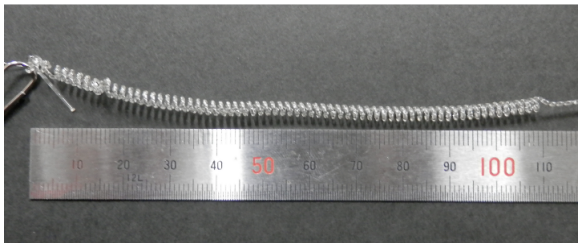

Fig. 3. TCPF used in the experiment.

III. Measurement experiment of displacement when driving the TCPF actuator

A. Fabrication of TCPF

According to Haines et al. [1], the TCPF actuator is fabricated by using two coiling methods. One method is over-twisting the polymer fiber, and the other is winding the fiber onto a mandrel after twisting the fiber until the time just before coiling. At the same temperature, the TCPF actuator fabricated using the former method can output larger force than that using the latter method. Meanwhile, the TCPF actuator fabricated using the latter method can output larger stroke. As this letter focuses on displacement sensor, we selected the latter method as the fabrication method.

The TCPF actuator used in the experiment is shown in Fig. 3. Similar to the author's previous works [24], [25], to drive the TCPF actuator by Joule heating, a 0.2 mm nichrome wire is first wound onto a nylon thread (TORAY, Ginrin 16-gou, diameter: 0.66 mm). With one end fixed and a 600 g weight hung at the other end, the thread was twisted until just before coiling. Then, we wound the twisted thread onto a mandrel with a diameter of 1.6 mm. To fix the thread in a coil shape, we heated the thread at 180 °C for 10 min by an automatic oven (DOV-450, AS-ONE).

B. Setup

We first evaluate the performance of the developed COF sensor when driving the TCPF actuator and then model the developed COF sensor. As this letter focuses on investigating whether the COF sensor is available when driving the TCPF actuator and changing the load, a practical model is established in this section.

The experimental environment around the TCPF is shown in Fig. 4. In the experiment, we attached a COF in parallel with the TCPF actuator. Because we supposed that the actuator unit with the developed COF sensor is driven in an air-cooling system, a cooling fan was used in the subsequent experiments. To prevent the TCPF actuator from melting by over-heating, its temperature was monitored using a thermography camera (OPTX180LTF05T090, Optris). For evaluation and modeling, the displacement measured by a laser range sensor (IL-300, KEYENCE) was used as the ground truth. The TCPF actuator was driven by the voltage input from a motor driver (DRI0017, DFRobot). The voltage reference was provided to the driver via Arduino UNO Rev3.

As the TCPF used herein has the large coil index, the weight, which can be hung in the experiment, decreases than that used in the fabrication. In all measurement experiments,

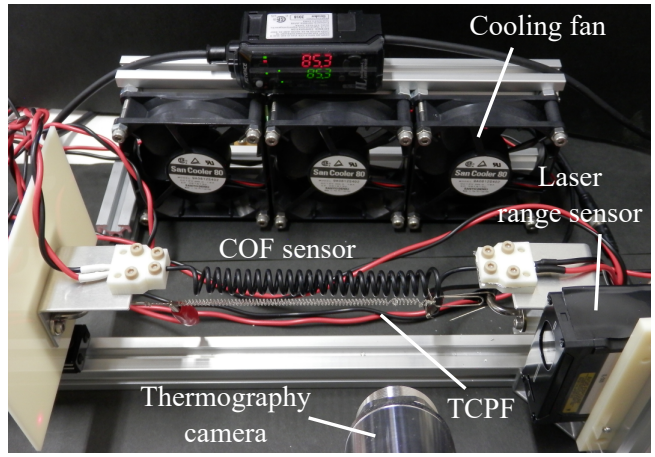

(a)

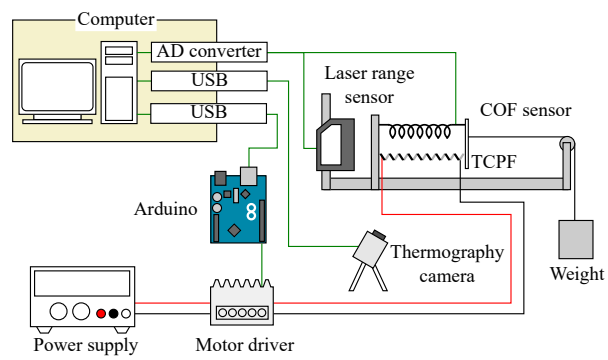

(b)

Fig. 4. Experimental environment. (a) Image showing the experimental environment around TCPF, and (b) overview of the experimental environment.

we hung a 100 g weight at the free end. The sampling time (excluding that of the thermography camera) was set as 10 ms, and that of the thermography camera was set as 100 ms. The ambient temperature was approximately 27°C.

To investigate the effect of coil diameter on the measurement, we tested three COFs shown in Table I. The coils were made of the same polyethylene-coated optical fiber (SH4001, Mitsubishi Chemical, diameter: 2.2 mm), and the number of active coils N_a of those were set to 23. To reduce the effect of the difference between the electronic components on the performance, we used the same electrical circuit, including the LED and the illuminance sensor. We conducted the measurement experiment three times per one COF.

C. Result and discussion

In the measurement experiment, the following voltage V_{ref} was inputted.

$$V_{\mathrm{in}} = \begin{cases} V_{\mathrm{ref}} & (\text{if } 0 \leq t < 30) \\ 0 & (\text{otherwise}) \end{cases} . \tag{1}$$

where V_{ref} is the positive reference voltage. In the measurement experiment, we set V_{ref} such that the TCPF temperature becomes approximately 90°C, namely, $V_{\mathrm{ref}} \simeq 10$ V. The experimental results of each coil are presented in Figs. 5 and

TABLE I

COIL-SHAPED OPTICAL FIBERS USED IN THE MEASUREMENT EXPERIMENT.

Coil	Coil diameter D [mm]	Proportional coefficient a_0 [V/mm]	Standard deviation deviation [$\times 10^{-2}$V]
A1	6.2	0.102757	0.977
A2	8.2	0.070958	1.146
A3	10.2	0.036425	1.195

6. For all trials, the relations between the voltage change ΔV and the displacement x are plotted in Fig. 7.

Fig. 7 shows that the displacement x of A3 is larger than that of A1 and A2, despite those temperature are almost the same; this is because of the spring stiffness of the COF. Indeed, according to Yip and Niemeyer [7], the TCPF actuator can be modeled as

$$m\ddot{x} + b\dot{x} + kx = c\Delta T \tag{2}$$

where m is the mass of the weight and b and k mean the damper and the spring stiffness of the TCPF actuator, respectively. c is the temperature coefficient, and ΔT denotes the temperature difference from the ambient temperature. As the COF is attached parallel to the TCPF actuator, (2) is rewritten as

$$m\ddot{x} + b\dot{x} + (k + k_{COF})x = c\Delta T \tag{3}$$

where k_{COF} is the spring stiffness of the COF and is given by

$$k_{COF} = \frac{Gd^4}{8N_a} D^{-3}, \tag{4}$$

where G means the modulus of transverse elasticity of the optical fiber. d and D denote the diameter of the optical fiber and the coil, respectively. As we used the same optical fiber and set N_a to be the same, k_{COF} is proportional to D^{-3}. By considering (3) at the static condition, the balance position x_e is given by

$$x_e = \frac{c\Delta T}{k + k_{COF}} \tag{5}$$

This indicates that the larger k_{COF} becomes, the smaller x_e is even at the same temperature. Since D of A3 is larger than that of A1 and A2, x_e of A3 increased, as shown in Fig. 7.

Additionally, Fig. 7 indicates that the slope depends on the coil diameter; one reason is owing to the rate of curvature radius. Indeed, the curvature radius of the coil is represented as

$$R = \frac{D}{2} + \frac{1}{2\pi^2 D}\left(\frac{x}{N_a}\right)^2. \tag{6}$$

By differentiating (6) by x, the rate of the curvature radius is written as

$$\frac{\mathrm{d}R}{\mathrm{d}x} = \frac{x}{\pi^2 N_a^2 D}, \tag{7}$$

As we set N_a to be the same, the rate mainly depends on the coil diameter $1/D$ when x is the same. The smaller D is, the larger the rate becomes.

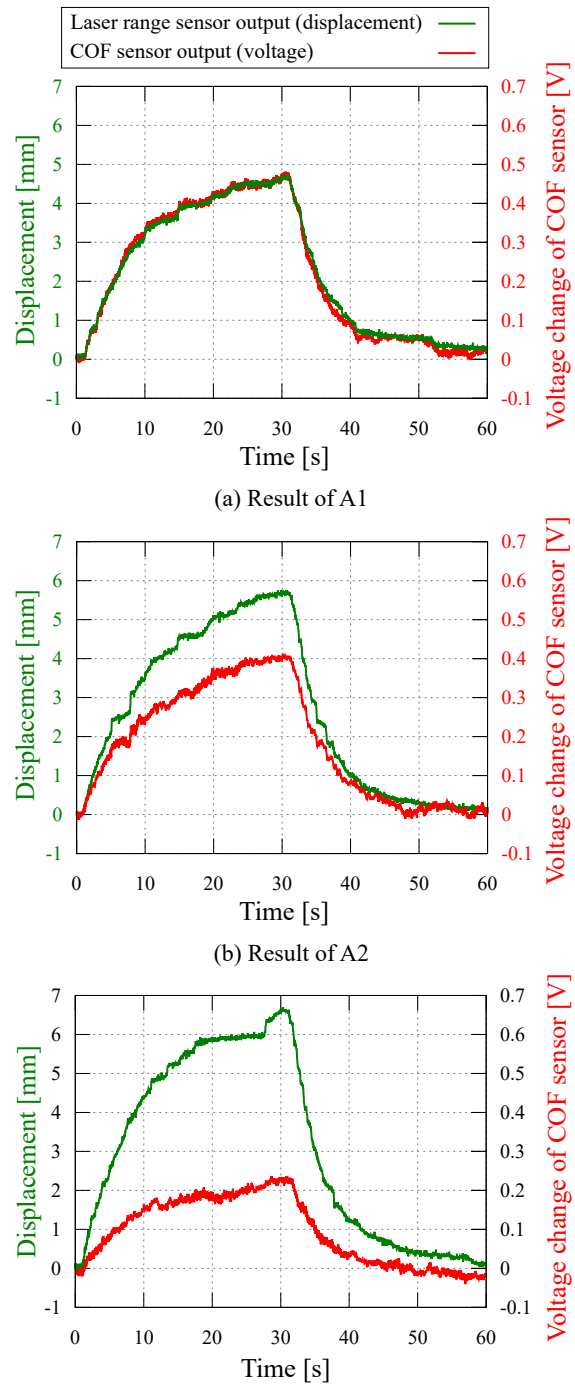

(a) Result of A1

(b) Result of A2

(c) Result of A3

Fig. 5. Experimental results of displacement and sensor output.

As Fig. 7 indicates that ΔV seems to be proportional to x in the range of measurement experiment, we modeled the relation between ΔV and x as follows:

$$\Delta V = a_0 x \tag{8}$$

where a_0 is the proportionality constant. From three experiments for each coil, each a_0 was identified, as shown in Table I. The identification process is detailed in Appendix A. Henceforth, we utilize A2 because of its sensitivity and stiffness.

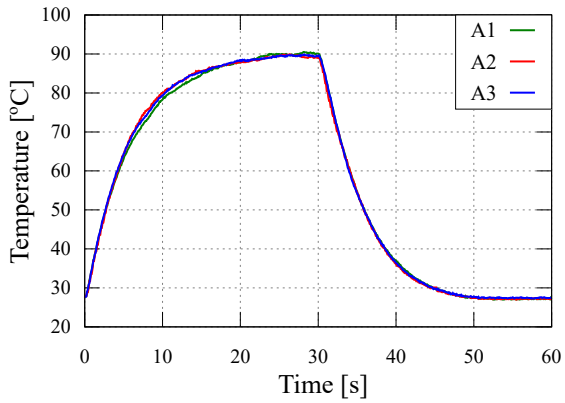

Fig. 6. Experimental results of temperature.

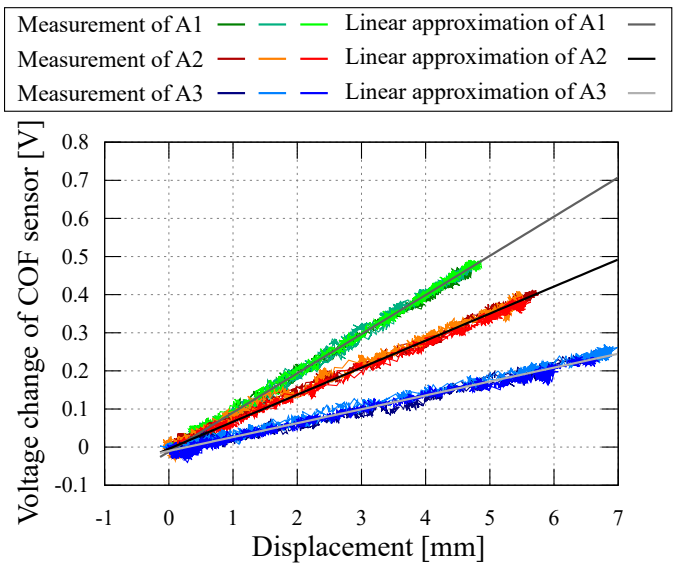

Fig. 7. Relation between displacement and output voltage difference.

IV. Control Experiment

A. Setup

To investigate the utility of the developed COF sensor when driving the TCPF actuator and changing the load, a control experiment using (8) was conducted. The experimental environment and the sampling times were the same as those used in the above experiment. In the previous works [12], [13], [25], the squared voltage is often employed to design the controller. For convenience, we used the proportional controller represented as follows:

$$V_{\mathrm{ctrl}}^2 = K_P(x_d - x) \tag{9}$$

where K_P is the proportional gain and x_d is the desired displacement. In the control experiments, V_{ctrl} is always positive. Additionally, to prevent the TCPF actuator from melting by over-heating, we set the upper voltage limit $V_{\max}$ [8], [12], [13], [25], [26], namely, $0 \leq V_{\mathrm{ctrl}} \leq V_{\max}$. In the following experiments, $V_{\max}$ and K_P were set as 12.0 V and 200.0 V^2/mm, respectively. From the preliminary experiment, when using the measurement by laser range sensor as x and hanging a 100 g weight, K_P was tuned such that convergence error was approximately 0.3 mm when

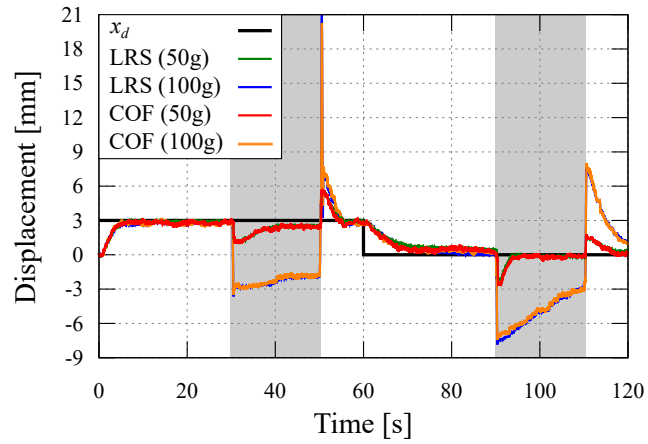

(a) Displacement

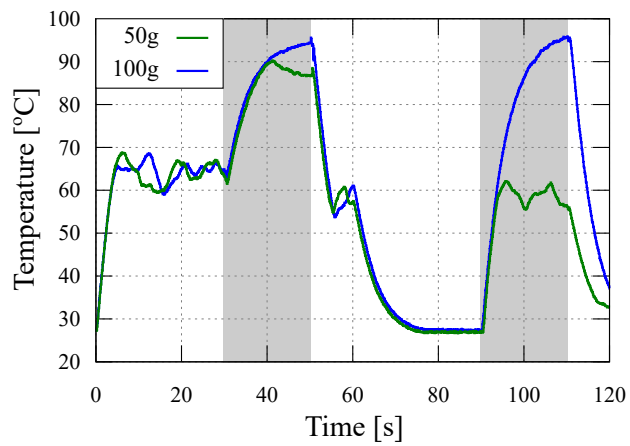

(a) Temperature

Fig. 8. Control results. The load is changed in the gray area. LRS and COF mean the displacement measured from the laser range sensor and from the developed COF, respectively. 50 g and 100 g in the legend denote the adding weight.

x_d =3 mm. Meanwhile, $V_{\max}$ was set to approximately 1.2 times of V_{ref} used in the measurement experiment. The sampling times of the control experiments were the same as those in the measurement experiments.

B. Results for the case of load change

In experiments, we set x_d as

$$x_d = \begin{cases} 3 & (\text{if } 0 \leq t < 60) \\ 0 & (\text{otherwise}) \end{cases} . \tag{10}$$

To evaluate the effect by the load change, the hung weight was changed. We first hung a 100 g weight, and then a 50 g or 100 g weight was added during 30 s–50 s and from 90 s–110 s. The control results are plotted in Fig. 8, and the input voltages are shown in Fig. 9.

First, we discuss the control result. From 0 s to 30 s, both the results converged in x_d. After the addition of weight, x left x_d, but immediately approached again. Because the input voltage, when adding a 100 g weight, saturated at this time, the error became large. Both results reconverged in x_d after removing the weight. After changing x_d, the TCPF temperature became the ambient temperature; nevertheless, x

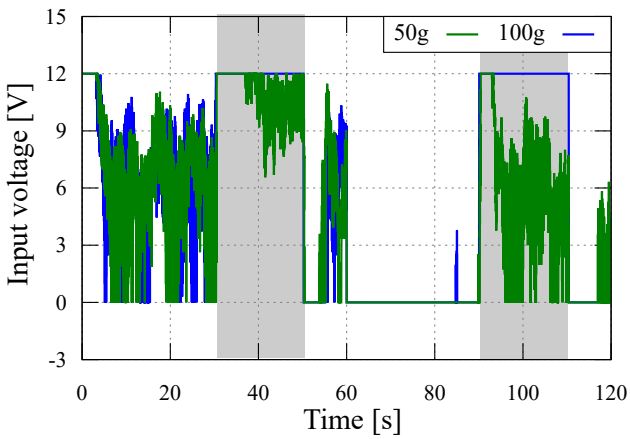

Fig. 9. Input voltage of each experiment.

of each experiment was different, indicating the occurrence of hysteresis. From 90 s to 110 s, the same weight was added again, causing both the results to approach x_d. After removing the weight again, both the results converged. These results show that the displacement of the actuator can be controlled by the output of the COF sensor.

Next, we focus on the relation between the displacement measured from the laser range sensor and from the developed COF sensor. This relation is presented in Fig. 10. The results indicate that the relation is almost the same despite each actuation behavior being different. This indicates that the actuation effect on the sensor output is small. Further, the COF sensor output is similar to the measured values from the laser range sensor, even if the weight was changed. When the displacement exceeds the range used in modeling, the relation departs from the modeled one mainly because of the modeling error. This indicates that the developed COF sensor has less dependence on the weight change in that range. Similarly, the developed COF sensor is available when hysteresis occurs.

C. Results for the case of the sinusoidal desired value

To evaluate the performance of the COF sensor when varying the desired value, we inputted the following sinusoidal desired value:

$$x_d = A_c \left(1 - \cos \frac{2\pi t}{t_c}\right), \tag{11}$$

where A_c and t_c denote the amplitude and the cycle of the sinusoidal input, respectively. In the experiments, A_c was set to 2 mm, and we employed two cycles, i.e., t_c =30 s and t_c =15 s.

The control results are presented in Fig. 11, and Fig. 10 shows the relation between the displacement measured from the laser range sensor and the developed COF sensor. These results demonstrate that the actuation effect on the sensor output is small, even when varying the desired value.

V. Conclusion

In this study, we proposed a low-cost COF displacement sensor to be used in an actuator unit combining a TCPF actuator with an air-cooling system. Based on the bending loss caused by the change in length of the COF, the displacement can be obtained from the output of the developed COF sensor. Experiments demonstrated that the developed COF sensor has less dependence on the TCPF actuation and the load change. Additionally, the developed COF sensor is available when hysteresis occurs.

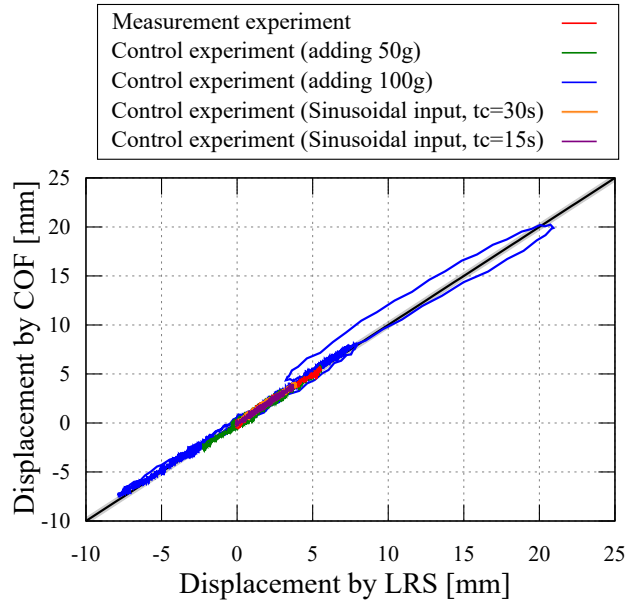

Fig. 10. Relation between the displacement measured by the laser range sensor (LRS) and by the developed COF sensor (COF). The gray area indicates 95% confidence interval obtained from the measurement experiments.

This study focused on investigating whether the developed COF sensor is available for sensing the displacement of the TCPF actuator. The control result shows that the modeling error arises out of the range used in modeling. This is because the nonlinearity of bending loss [22], [23] cannot be ignored when the displacement per coil is larger. Therefore, deriving a detailed model based on the optical fiber's property is one of the future works. In addition, the detailed model enables us to establish the design procedure of the COF sensor.

Acknowledgement

A Grant-in-Aid for Challenging Research, Organization of Fundamental Research, Tokyo Institute of Technology.

Appendix

A. Detail of identification process

This letter identified the model parameter a_0 by the linear least-squares method. To consider the offset variation of each trial, the following model is used in the identification process instead of (8).

$$\Delta V = a_0 x + a_1. \tag{12}$$

By using (12), we minimize the following evaluation function.

$$E = \frac{1}{2} \sum_{i}^{N_d} \left(\Delta \tilde{V}_i - \Delta \hat{V}_i\right)^2, \tag{13}$$

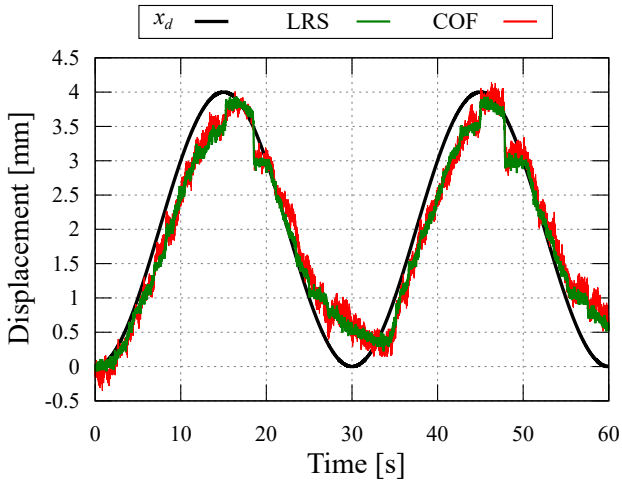

(a) t_c = 30s

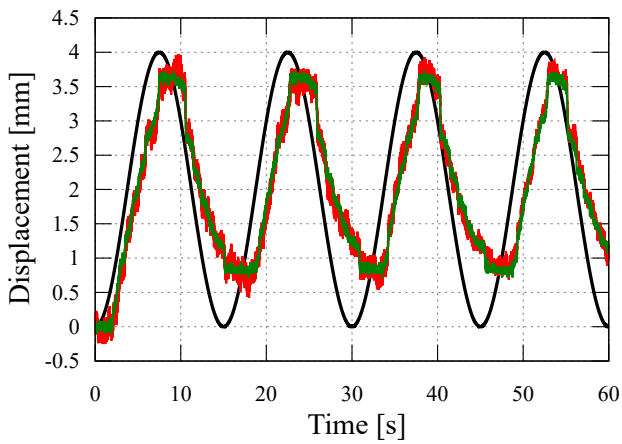

(b) t_c = 15s

Fig. 11. Control results for the sinusoidal desired value. LRS and COF mean the displacement measured from the laser range sensor and from the developed COF, respectively.

where $\Delta\tilde{V}_i$ means i-th measurement of ΔV, and $\Delta\hat{V}_i$ is i-th predicted value of ΔV obtained by (12). N_d denotes the total number of data per trial. After obtaining a_0 and a_1 of each trial by minimizing E, we average a_0 and a_1 of all trials.

References

[1] C. S. Haines et al., "Artificial Muscles from Fishing Line and Sewing Thread," Science, vol. 343, no. 6173, pp. 868–872, Feb. 2014.

[2] M. Hiraoka et al., "Power-efficient low-temperature woven coiled fibre actuator for wearable applications," Scientific Reports, vol. 6, 36358, Nov. 2016.

[3] K. Kim et al., "Double Helix Twisted and Coiled Soft Actuator from Spandex and Nylon," Advanced Engineering Materials, vol. 20, no. 11, 1800536, Aug. 2018.

[4] S. Tawfick and Y. Tang, "Stronger artificial muscles, with a twist," Science, vol, 365, no. 6449 pp. 125–126, Jul. 2019.

[5] L. Wu et al., "Nylon-Muscle-Actuated Robotic Finger," in Proc. of SPIE 9431, San Diego, CA, USA, Mar. 2015, 94310I.

[6] H. Song and Y. Hori, "Force control of twisted and coiled polymer actuators via active control of electrical heating and forced convective liquid cooling," Advanced Robotics, vol. 32, no. 14, pp. 736–749", 2018.

[7] M. C. Yip and G. Niemeyer, "High-Performance Robotic Muscles from Conductive Nylon Sewing Thread," in Proc. of the 2015 IEEE Int. Conf. on Robotics and Automation, Seattle, WA, USA, May 2015, pp. 2313–2318.

[8] K. Takagi et al., "Position control of Twisted and Coiled Polymer Actuator Using a Controlled Fan for Cooling," in Proc. of SPIE, vol. 10163, Portland, OR, USA, Mar. 2017, 101632V.

[9] J. van der Weijde, et al., "Self-Sensing of Deflection, Force, and Temperature for Joule-Heated Twisted and Coiled Polymer Muscles via Electrical Impedance," IEEE/ASME Transactions on Mechatronics, vol. 22, no. 3, pp. 1268–1275, Jun. 2017.

[10] A. Abbas and J. Zhao, "A Physics Based Model for Twisted and Coiled Actuator," in Proc. of the 2017 IEEE Int. Conf. on Robotics and Automation, Singapore, May 2017, pp. 6121–6126.

[11] A. Abbas and J. Zhao, "Twisted and Coiled Sensor for Shape Estimation of Soft Robots," in Proc. of the 2017 IEEE/RSJ Int.l Conf. on Intelligent Robots and Systems, Vancouver, BC, Canada, Sep. 2017, pp. 482–487.

[12] K. Tahara et al., "Rotational Angle Control of a Twisted Polymeric Fiber Actuator by an Estimated Temperature Feedback," IEEE Robotics and Automation Letters, vol.4, no.3, pp.2447–2454, 2019.

[13] R. Hayashi et al., "Two-degree-of-freedom Control of The Rotational Angle for a Twisted Polymeric Fiber Actuator by Temperature Estimation," IEEE Robotics and Automation Letters, vol.4, no.3, pp.2561–2567, 2019.

[14] J. van der Weijde, H. Vallery, and R. Babuška, "Closed-Loop Control Through Self-Sensing of a Joule-Heated Twisted and Coiled Polymer Muscle," Soft Robotics, vol. 6, no. 5, pp. 621–630, 2019.

[15] J. Zhang et al., "Modeling and Inverse Compensation of Hysteresis in Supercoiled Polymer Artificial Muscles," IEEE Robotics and Automation Letters, vol 2, no. 2, pp. 773–780, 2017.

[16] H. Tanizaki et al., "Experimental investigation of temperature-dependent hysteresis of fishing-line artificial muscle (twisted and coiled polymer fiber) actuator," in Proc. of SPIE 10966, Electroactive Polymer Actuators and Devices (EAPAD) 2019, Denver, CO, USA, Mar. 2019, 109660U.

[17] B. P.R. Edmonds and A. L. Trejos, "Design of an Active Cooling System for Thermally Activated Soft Actuators," in Proc. of 2019 IEEE 16th International Conference on Rehabilitation Robotics, Toronto, Canada, Jun. 2019, pp. 368–373.

[18] C. Xiang et al., "The design, hysteresis modeling and control of a novel SMA-fishing-line actuator," Smart Materials and Structures, vol. 26, no. 3, 037004, Feb. 2017.

[19] D. Bombara et al., "Self-Sensing for Twisted String Actuators Using Conductive Supercoiled Polymers," in Proc. of the ASME 2019 Conference on Smart Materials, Adaptive Structures and Intelligent Systems, Louisville, KY, USA, Sep. 2019, SMASIS2019-5587.

[20] R. Xu, A. Yurkewich, and R. V. Patel, "Curvature, Torsion, and Force Sensing in Continuum Robots Using Helically Wrapped FBG Sensors," IEEE Robotics and Automation Letters, vol.1, no.2, pp.1052–1059, 2016.

[21] S. Wakimoto et al., "Proposal and prototype of a McKibben artificial muscle with an optical fiber for sensing displacement (in Japanese)," in Proc of JSME annual Conf. on Robotics and Mechatronics, 1P1-G10, 2019.

[22] L. Meng et al., "An investigation in the influence of helical structure on bend loss of pavement optical fiber sensor," Optik, vol. 183, pp. 189–199, Feb. 2019.

[23] D. Marcuse, "Curvature loss formula for optical fibers," J. of the Optical Society of America, vol. 66, no. 3, pp. 216–220, Mar. 1976.

[24] K. Masuya et al., "Modeling Framework for Macroscopic Dynamics of Twisted and Coiled Polymer Actuator Driven by Joule Heating Focusing on Energy and Convective Heat Transfer," Sensors and Actuators A: Physical, vol 267, pp. 443–454, 2017.

[25] K. Masuya et al., "Feedforward Control of Twisted and Coiled Polymer Actuator based on a Macroscopic Nonlinear Model Focusing on Energy," IEEE Robotics and Automation Letters, vol.3, no.3, pp.1824–1831, 2018.

[26] M. Suzuki and N. Kamamichi, "Displacement control of an antagonistic-type twisted and coiled polymer actuator," Smart Materials and Structures, vol. 27, no. 3, 035003, Jan. 2018.